Effect of taper on fundamental aeroelastic behaviors of super-tall buildings

Yong Chul Kim [*1], Yukio Tamura [2a] and Sung-won Yoon [3b]

[1]*Wind Engineering Research Center, Tokyo Polytechnic University, 1583 Iiyama, Atsugi 242-0297, Japan*
[2]*School of Civil Engineering, Beijing Jiaotong University, 3 Shangyuancun, Xizhimenwai, Beijing 100044, P.R. China*
[3]*School of Architecture, Seoul National University of Science and Technology, 232 Gongneung-ro Nowon-gu, Seoul 139-743, Korea*

Abstract. Aeroelastic wind tunnel experiments were conducted for conventional and tapered super-tall building models to investigate the effect of taper on fundamental aeroelastic behaviors in various incident flows. Three incident flows were simulated: a turbulent boundary-layer flow representing urban area; a low-turbulent flow; and a grid-generated flow. Results were summarized focusing on the effect of taper and the effect of incident flows. The suppression of responses by introducing taper was profound in the low-turbulence flow and boundary-layer flow, but in the grid-generated flow, the response becomes larger than that of the square model when the wind is applied normal to the surface. The effects of taper and incident flows were clearly shown on the normalized responses, power spectra, stability diagrams and probability functions.

Keywords: wind tunnel experiment; aeroelastic behavior; taper; low-turbulence flow; grid-generated flow; boundary-layer flow

1. Introduction

In many cases, wind loads are considered as the governing horizontal loads in the structural design of modern super-tall building projects, and it is well known that across-wind responses become much greater than along-wind responses with increasing building heights. Furthermore, the onset velocity of vortex-induced vibration can be within the design wind speed for super-tall buildings with large aspect ratios, that is, larger than 8 (Kawai 1995). The suppression of across-wind responses have thus been an important issue for wind engineers over the last two decades. Lots of attempts have been made to suppress across-wind responses by changing building shapes. As wind loads largely depend on building shapes as well as structural characteristics, i.e., mass distribution, stiffness, and structural damping ratio, studies on aerodynamic modifications have been one of the most challenging issues in wind-resistant design of modern super-tall buildings

∗Corresponding author, Associate Professor, E-mail: gentle95@gmail.com
[a] Honorary Professor, E-mail: yukio@arch.t-kougei.ac.jp
[b] Professor, E-mail: swyoon@seoultech.ac.kr

and slender structures. Aerodynamic modifications include taper, set-back, twisting and corner modifications like corner cut, corner recess and/or corner rounding, and comprehensive studies on various aerodynamic modifications have been reported by Tanaka *et al.* (2012) and Kim and Kanda (2010, 2013).

The effects of various incident flows on aeroelastic behaviors have been examined by many researchers mostly only for conventional (super-) tall buildings and slender structures. The square cross-section has been examined in depth since the work by Parkinson and Smith (1964). The effects of turbulence on vortex-induced vibrations of square/rectangular (super-) tall buildings or slender structures have been studied, and different aeroelastic behaviors due to different incident flow conditions have been reported (Novak and Davenport 1970, Kwok and Melbourne 1980, Belloli *et al.* 2011, Belloli *et al.* 2014). But at present it is generally accepted that the effects of the incident flows on vortex-induced vibrations of square/rectangular super-tall buildings have not been fully understood. A comprehensive review of these studies can be found in Naudascher and Rockwell (2005). Due to rapid development of computer industries, recent improvements in computational fluid dynamics techniques are very promising. However, wind tunnel experiments have been believed as the most reliable methods for examining the aeroelastic behaviors of super-tall buildings and slender structures (Pozzuoli *et al.* 2013, Huang *et al.* 2013, John *et al.* 2011).

Although many studies have been carried out to determine how shape modifications suppress vortex-induced vibrations, most of them have focused on corner modifications (Kawai 1995, Carassale *et al.* 2013) and limited numbers of researches on aeroelastic behaviors of tapered super-tall buildings have been found (Kim *et al.* 2008). Moreover, there have been few reports on the effects of incident flow conditions on the aeroelastic behavior of tapered super-tall building. Therefore, in the present study, the effect of taper on fundamental aeroelastic behavior was investigated in various incident flows. Three incident flows were simulated: a turbulent boundary-layer flow representing urban area; a low-turbulent flow; and a grid-generated flow. Even though the low-turbulence flow and the grid-generated flow may not be encountered frequently in the super-tall building projects, these flow conditions were employed for the better understanding of the aeroelastic effect of taper. The effect of taper and various incident flows were summarized in terms of normalized responses, power spectra, stability diagrams, probability functions, and so on.

2. Aeroelastic wind tunnel experiment

Aeroelastic wind tunnel experiments were conducted in an open-circuit turbulent boundary-layer wind tunnel. Fig. 1 shows the profiles of the mean wind speed and turbulence intensity of three incident flows. No turbulence-generating apparatuses and spires were used for the simulation of low-turbulence flow shown in Fig. 1(a). But, because of friction with the wind tunnel floor, there are slight slopes in mean wind speed and turbulence intensity up to 0.2 m, which corresponds to about $0.36H$. The turbulence intensity at model height is about 0.3%. Grid-generated flow was simulated by placing a grid 0.9 m upstream of the experimental models, as shown in Fig. 1(b) and Fig. 2(a). The grid size is 0.09 m×0.09 m, and the grid was fixed to the wind tunnel wall and floor during the experiments. In the grid-generated flow, there is a slight inverse slope in mean wind speed up to about $0.36H$, but the turbulence intensities are reasonably constant throughout the height. The turbulence intensity at model height of grid-generated flow was adjusted to the same value as that of boundary-layer flow ($I_{u,H} \approx 10\%$). Boundary-layer flow was simulated using spires and various-sized roughness elements, as shown in Figs. 1(c) and 2(b). The power-law index of

turbulent boundary-layer flow is 0.27, which represents an urban area flow. The turbulence intensity at model height was about $I_{u,H} \approx 10\%$. In urban area flow condition, the turbulence intensity at 448m in full scale is about 10% based on the current Japanese code (AIJ-RLB (2004) 2004). Different mean wind speeds at model height ranging between 0 m/s and about 7 m/s were used, but in the experiments, the mean wind speeds were limited by excessive vibrations of the experimental models.

Figs. 2(a) and 2(b) shows the setting of experimental models in a grid-generated flow and boundary-layer flow. The total volume of the square and tapered models was set the same. Displacements were measured at the bottom of the experimental models by laser displacement sensors in the X and Y directions (Fig. 2(c)), and these displacements were converted to tip displacements. Considering the double-symmetry shape of models, wind directions from 0° to 45° were considered. The sampling frequency of the laser displacement sensors was 510 Hz, and the measurement time was adjusted such that 10 10-min samples for boundary-layer flow and 5 10-min samples for a low-turbulence and grid-generated flow were obtained. The natural frequency of a reinforced concrete building was assumed ($n_0 = 67/H$) (Tamura 2012), and the natural frequencies (n_{X0} and n_{Y0}) and damping ratios (ζ_X and ζ_Y) were adjusted by means of the spring stiffness and magnetic field at the bottom of the experimental models.

The natural frequencies and the damping ratios were obtained from free vibration signals and are given in Table 1 with other parameters. In current experimental condition, the effects of higher modes cannot be observed. But for displacements the effects of higher modes are hardly observed for the super-tall buildings (Tanaka *et al.* 2013), only the effect of the first mode was focused on in the present study.
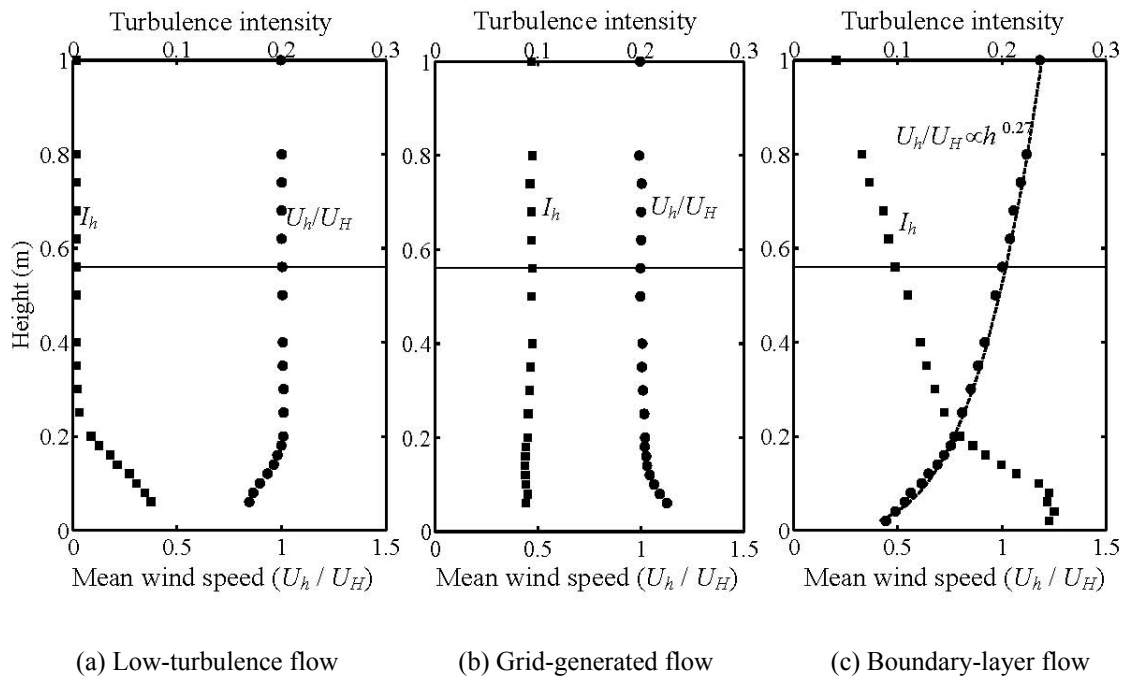

(a) Low-turbulence flow   (b) Grid-generated flow   (c) Boundary-layer flow

Fig. 1 Profiles of mean wind speed and turbulence intensity

The Reynolds numbers ($Re=BU_H/v$) defined by width of the square model, mean wind speeds at model height and kinematic viscosity ($v=1.45\times10^{-5}m^2/s$) ranged from approximately 5.1×10^3 to 7.1×10^4 and the Scruton number ($Sc=2m\zeta/\rho D^2$) is about 2.2, where m is mass per unit height, ρ is air density, and D is depth of the square model. The blockage ratio is about 1%, so no corrections were made to the experimental data.

(a) Tapered model under grid-generated flow   (b) Square model under boundary-layer flow
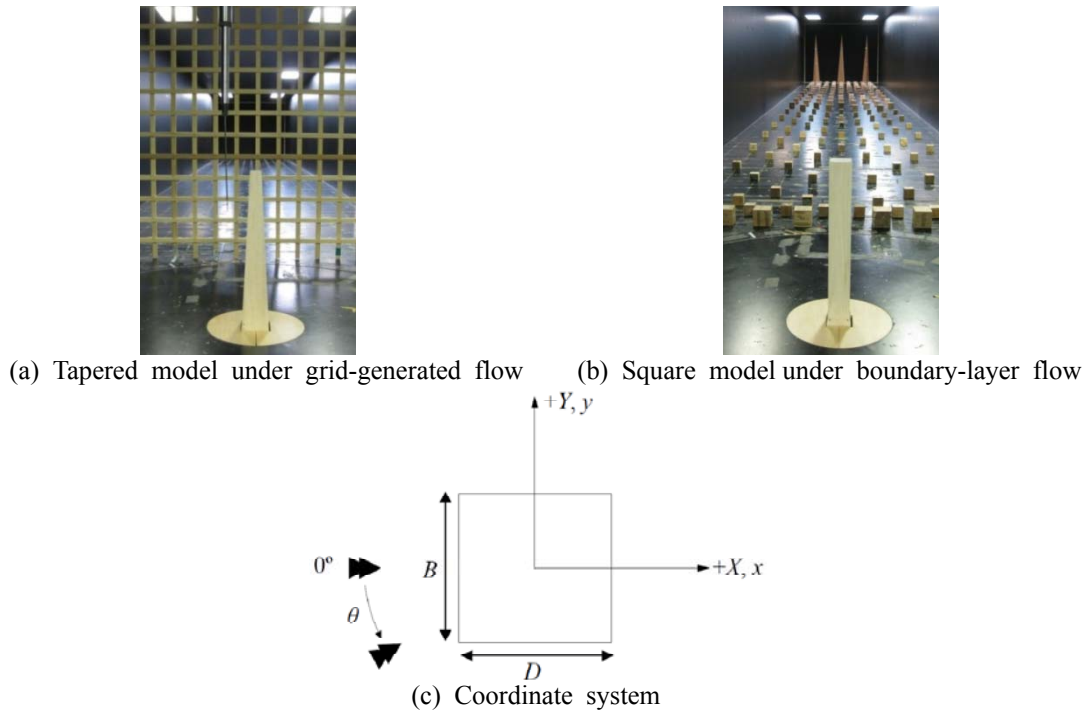
(c) Coordinate system

Fig. 2 Setting of experimental models and definition of coordinate system

Table 1 Parameters of experimental models

	Square model	Tapered model
Bottom width (=Depth) (B (=D), m)	56	77.6
Top width (=Depth) (B (=D), m)	56	31.2
Height (H, m)	448	
Total volume (m^3)	About 1.4×10^6	
Target natural frequency (n_{X0} / n_{Y0}, Hz)	0.15 / 0.15	
Target damping ratio (ζ_X / ζ_Y, %)	0.8 / 0.8	
Reynolds number (by B and U_H)	$5.1\times10^3 \sim 7.1\times10^4$	
Mode shape	1st linear mode	

3. Experimental results and discussion

3.1 Normalized response

Figs. 3 and 4 show normalized responses in the *Y* direction in terms of normalized velocities for different incident flows. The ordinate indicates the normalized fluctuating tip displacement (σ_y/B), and normalized velocity is defined by mean wind speed at model height, natural frequency, and width of the square model ($U_H^*=U_H/n_0B$).

In Fig. 3(a) for the square model for the low-turbulence flow, the vortex-induced vibrations were shown for the normalized velocity larger than $U_H^*\approx8$ when wind directions were between 0° and 10°. For these wind directions, the largest normalized response increases with wind direction, and the normalized velocity for the largest normalized response also increases. When wind direction becomes 15° or 20°, the normalized responses decrease suddenly, and again increase slowly for wind directions larger than 20°. A similar tendency for sudden decrease of response for low-turbulence flow can be found in Kwok and Melbourne (1980).
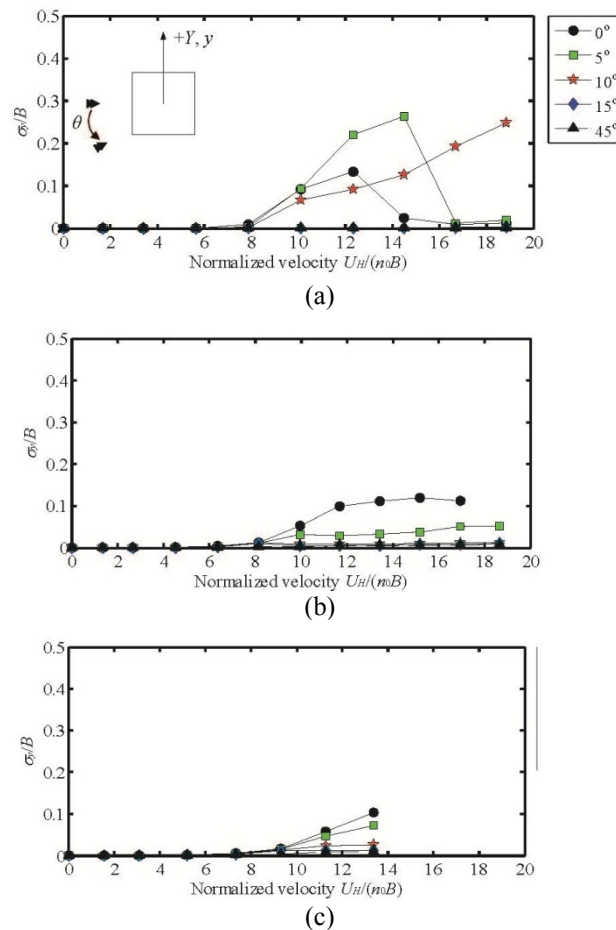

(a)

(b)

(c)

Fig. 3 Normalized response in *Y* direction of square model (a) Low-turbulence flow, (b) Grid-generated flow and (c) Boundary-layer flow

The variations of the normalized responses for the grid-generated flow are shown in Fig. 3(b), which are totally different from those for the low-turbulence flow shown in Fig. 3(a). The normalized velocity at which the normalized response started to increase is slightly smaller than that for the low-turbulence flow, and large responses were found for wide ranges of normalized velocity for the wind direction of 0°. The normalized responses become constant for normalized velocities larger than $U_H{}^*=12$ for the wind direction of 0° and $U_H{}^*=10$ for the wind direction of 5°. When wind direction is larger than 10°, the normalized responses show almost the same values.

The normalized responses for the boundary-layer flow are shown in Fig. 3(c). In the boundary-layer flow, the normalized responses are very small and increase monotonically for the current experimental conditions. The normalized velocity at which the normalized response started to increase is about $U_H{}^*\approx7$ and the normalized responses for wind directions greater than 15° are almost the same.
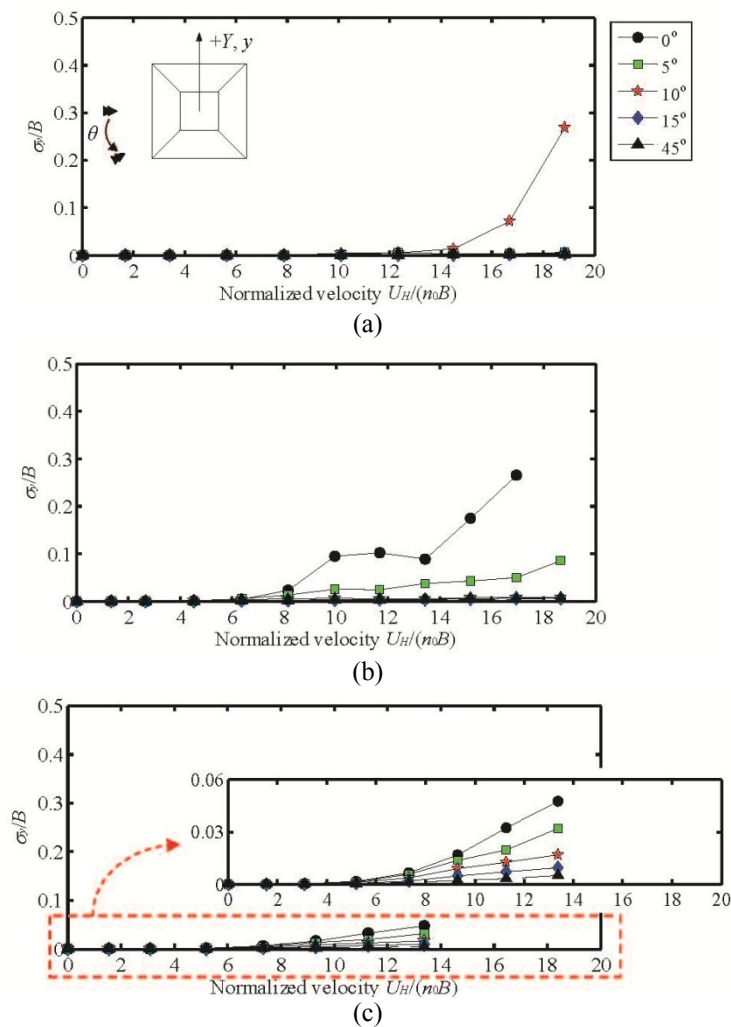

Fig. 4 Normalized response in *Y* direction of tapered model (a) Low-turbulence flow, (b) Grid-generated flow and (c) Boundary-layer flow

The variations of the normalized responses of the taper model are shown in Fig. 4. In low-turbulence flow (Fig. 4(a)), when the aerodynamic modification of taper was implemented, the normalized response decreases significantly for wind directions of 0° and 5°, showing no vortex-induced vibrations when compared with Fig. 3(a). For the wind direction of 10°, vortex-induced vibrations were shown, but the normalized velocity for the vortex-induced vibration is much higher than that of the square model ($U_H^* \approx 14$). This implies that by introducing taper the normalized responses were greatly suppressed at small wind directions, and the vortex-induced vibrations were shown for the specific wind direction which is not normal to the surface. And the normalized velocity for the vortex-induced vibrations becomes higher.

But in the grid-generated flow (Fig. 4(b)), suppression of the responses cannot be expected, showing larger responses than those of the square model for the normalized velocity $U_H^* > 14$ for the wind direction of 0°. This trend is only found for the grid-generated flow, meaning that for the flow conditions with very small slope in mean wind speed and with moderate turbulence intensity, the introduction of taper may cause worse results, especially for the wind normal to the surface with large wind speed. The variation for wind directions larger than 15° was similar to that of the square model.

In boundary-layer flows the normalized responses increase monotonically, and moderate suppression of normalized responses is observed as shown in Fig. 4(c). The variation of normalized responses for wind directions larger than 15° is very small, and any vortex-induced vibrations were not found for both square and tapered model

The combined effects of increasing wind directions and incident flows can be explained by the degree of entrainment as shown in Fig. 5 (Kwok and Melbourne 1980). Fig. 5 shows mean streamlines around the models. At small wind directions, there is a partial reattachment of the separated shear layer on the side surface in low-turbulence flow, but at the same wind directions, more substantial reattachment is expected in the grid-generated flow (Fig. 5(a)). This is believed to be caused by the increase in the rate of entrainment and a decrease in the radius of curvature of the separated shear layers associated with the level of turbulence in the incident flow. This means that in the grid-generated flow, the permanent reattachment occurs at smaller wind directions than low-turbulence flow (Figs. 5(b) and 5(c)), and this can explain the large decrease in the normalized responses at the wind directions of 5° and 10° in the grid-generated flow. And the normalized responses in the grid-generated flow are similar to or larger than those in the low-turbulence flow at the wind direction of 0°, and this result comes from the promotion of the entrainment of the separated shear layer by presence of turbulence in the incident flow, approaching the separated shear layer to the side surface of building (Fig. 5(a)). Together with the presence of turbulence, the building shape of taper seems to have an inverse effect to increase the responses at the wind direction of 0° as shown in Fig. 4(b).

Fig. 6 shows the normalized responses in the *X* direction for various incident flows for the wind direction of 0°. Basically, as the responses in *X* direction are mainly resulted from the turbulence in the incident flows, the responses for grid-generated flow and boundary-layer flow are larger than those of low-turbulence flow, and increase monotonically for both the square and tapered models. But for the square model, the response in the low-turbulence flow suddenly increase near the normalized velocity of $U_H^* \approx 8$, showing a similar trend to that in the *Y* direction. For this normalized velocity ranges, the correlations between the responses in the *X* and *Y* directions are very high as shown in Fig. 7(a). The responses of the tapered model are smaller than those of the square model, and increase monotonically as the square model.

For other wind directions, the normalized responses increase monotonically with the

normalized velocities regardless of the incident flows and building shapes, showing smaller values at large wind directions. The normalized responses of the tapered model are smaller than those of the square model as expected.

For references, the projected areas of the square and tapered models are almost the same at the wind direction of 0°.

3.2 Cross-correlation coefficient

The cross-correlation coefficients between the responses in the X and Y directions were calculated and those of small wind directions are shown in Fig. 7.

In low-turbulence flow, the cross-correlation coefficients of the square model (SQ) decreased with normalized velocity up to $U_H^*{\approx}8$, but they became very large for normalized velocities from $U_H^*{\approx}8$ to 14, especially showing over 0.9 for the wind direction of 10°. The tapered model (TP) showed a similar trend up to the normalized velocity of $U_H^*{\approx}8$, but the cross-correlations become very small and show constant negative values for the higher normalized velocity.
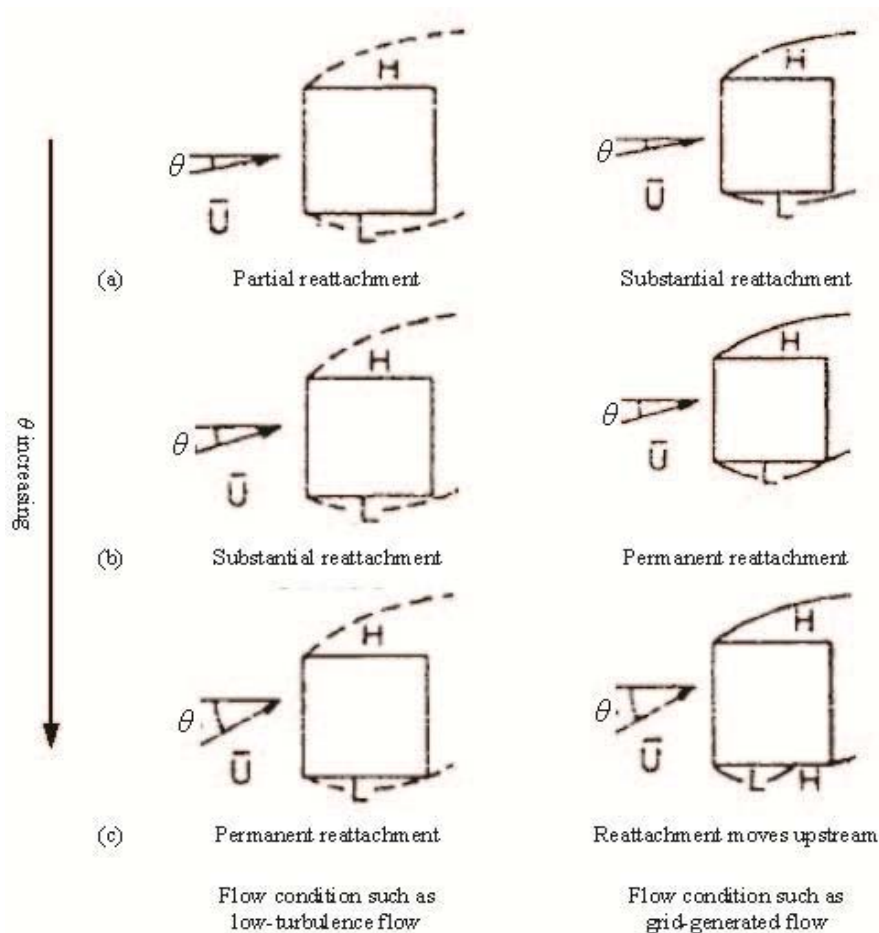

Fig. 5 Effects of turbulence intensity and wind direction (after Kwok and Melbourne 1980, L means lower pressure (larger absolute value) and H means higher pressure (smaller absolute value))

The cross-correlation coefficients in grid-generated flow were generally small and show constant positive values for wide ranges of normalized velocity. But for specific ranges, the cross-correlations for the tapered model were larger than those for the square model, i.e., the normalized velocities between $U_H^* \approx 8$ and $U_H^* \approx 12$ for the wind direction of 0°, and the normalized velocities over $U_H^* \approx 14$ for the wind direction of 5°.

In boundary-layer flows, the cross-correlations decreased with normalized velocity up to $U_H^* \approx 5$, and they became nearly constant and negative after that for the square and tapered models.

From the above discussions, the effects of incident flows are clearly identified, and the effect of taper in various incident flows can also be well understood. Thus, the flow conditions should be identified thoroughly for various wind directions in tall building projects. The highest gradient heights prescribed in current wind-load standards and codes of practice are mostly less than 600 m, and many mega-tall buildings higher than 600 m are under construction and will be constructed. This means that the upper part of the buildings can be exposed to grid-generated flow or low-turbulence flow. Furthermore, aerodynamic modifications like taper and setback are frequently used in modern tall buildings. Thus, aeroelastic behavior should be examined carefully using both full-scale and section models.
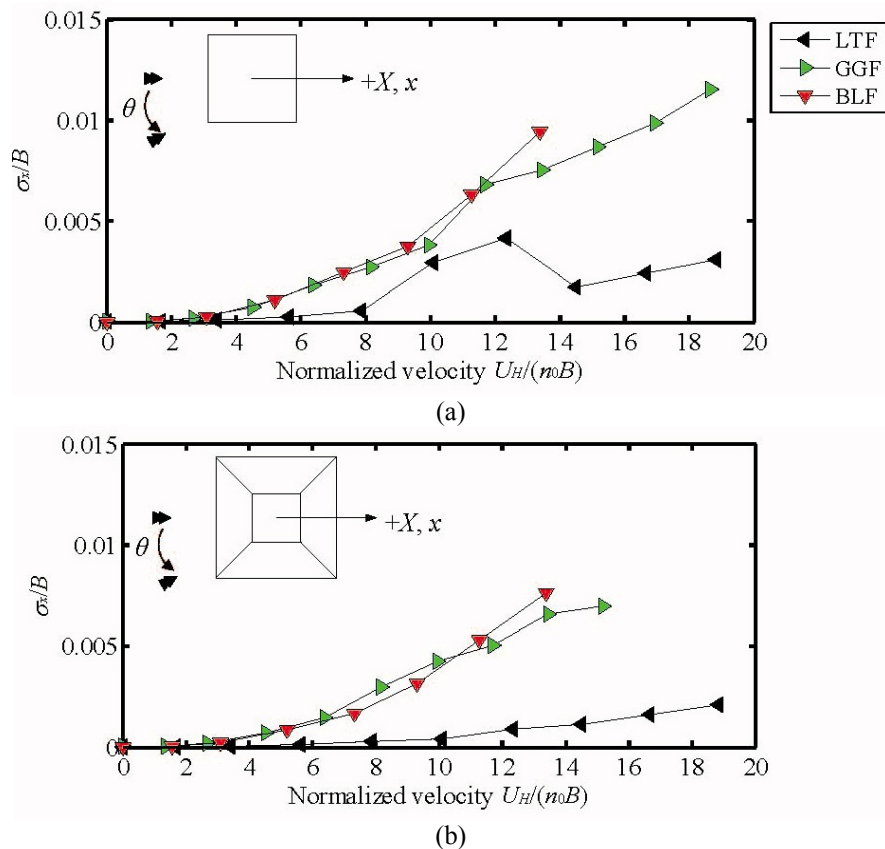

Fig. 6 Normalized response in *X* direction for various incident flows when the wind direction is 0° (a) Square model and (b) Tapered model
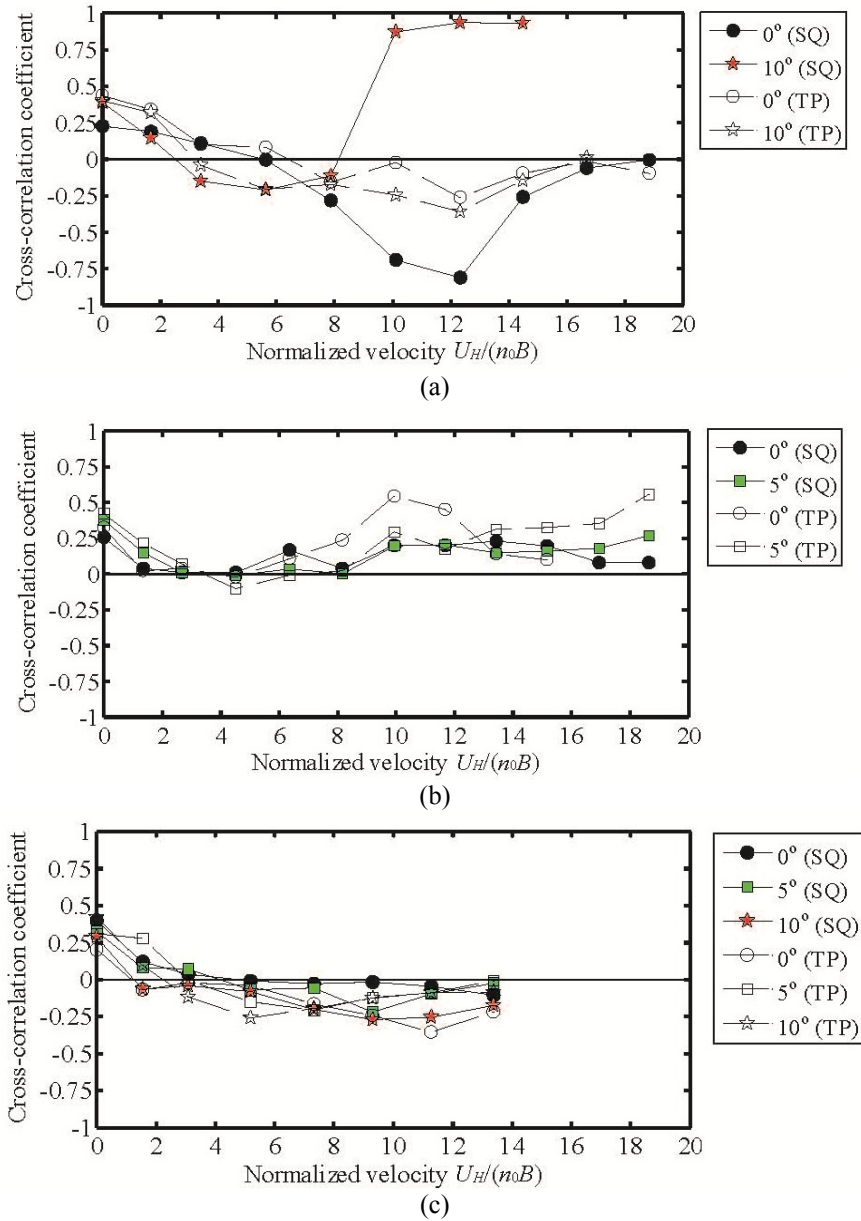
Fig. 7 Cross-correlation coefficients between responses in X and Y directions for small wind directions
(SQ means square model and TP means tapered model) (a) Low-turbulence flow, (b) Grid-
generated flow, (c) Boundary-layer flow

And as mentioned before, when a tapered super-tall buildings constructed in the area where the
slope in mean wind speed is very small and turbulence intensity is moderate, a tapered building
shape results in worse aeroelastic behaviors, especially for high-speed wind normal to the surface.

3.3 Stability diagram

From the relationship between normalized response in the *Y* direction and the normalized velocity shown in Figs. 3 and 4, stability diagrams were produced, as shown in Fig. 8. The three threshold levels of the responses, σ_y/B=1/100, 150, and 200 were considered, and these threshold levels were determined to be similar to those of Kawai (1995). The region under the line of a certain threshold level indicates a stable region and that above the line indicates an unstable region. The region inside the circles also indicates an unstable region. The unstable region becomes wider for the smaller threshold level, as expected.

In the low-turbulence flow in Fig. 8(a), there are no unstable regions when the wind direction is larger than 15° for the square model, and there is little difference in stability diagram for the threshold levels of σ_y/B=150 and 200. For the tapered model, the unstable region was found near the wind direction of 10° and at the larger normalized velocity shown in Fig. 4(a), showing a very different trend from the square model. There is little difference in unstable region for the threshold levels of σ_y/B=100 and 150.

The effects of turbulence in incident flow can again be confirmed in the stability diagram shown in Fig. 8(b). With the introduction of moderate turbulence, the unstable region greatly increased for the square and tapered models, and the unstable region of the square model is larger than that of the taper model for the considered wind directions. But when the threshold level is low (σ_y/B=200) and for small wind directions, the tapered model becomes unstable for smaller normalized velocity rather than the square model.

In the boundary-layer flow (Fig. 8(c)), by introducing the profile in mean wind speed and turbulence intensity, the unstable region becomes wider for the square model, and the unstable regions for the threshold levels of σ_y/B=150 and 200 become similar. But for the tapered model the unstable region becomes significantly small, showing no unstable regions when the wind direction is larger than 5° or 10°. The stability diagram is very similar to that of the square model in the low-turbulence flow. When the design criteria of tip displacement is assumed to be near σ_y/B=100 which corresponds to σ_y/H=800, the normalized design velocity ranges roughly from $U_H{}^*\approx7$ to 10 for the wind directions from 0° to 30° for the square model, and about $U_H{}^*\approx12$ from 0° to 5° for the tapered model, ascertaining again the effect of taper on suppressing responses for wide ranges of wind directions.

3.4 Power spectrum of tip displacement

Power spectra of tip displacements were calculated to examine the condition of vortex shedding and to understand the normalized response in detail. The power spectra of the square and tapered model in the low-turbulence flow are shown in Figs. 9 and 10, respectively, for small wind directions.

Values near the peak at natural frequency (dotted vertical line) are the powers of the peaks. For the square model in Fig. 9, two clear peaks are observed; one corresponds to a vortex shedding frequency n_s (▼ in the figure) and the other is a natural frequency of the system n_0 (● in the figure). For low normalized velocities, that is, $U_H{}^*$<5.6, the peak by vortex shedding is larger than that for the natural frequency, and for high normalized velocities, the peak for the natural frequency is much larger than that for vortex shedding. For the normalized velocity near $U_H{}^*\approx10$, only one peak is observed, meaning lock-in excitation. As the normalized velocity increases, the increase of vortex shedding frequency is clearly seen, and the vortex shedding frequencies are

found roughly up to the wind direction of 15°. Similar discussions can be made for the tapered model shown in Fig. 10, but it was found that the peaks by vortex shedding were greatly suppressed. For the normalized velocities where vortex-induced vibrations were found, the powers of natural frequencies greatly increased, as pointed out by Kawai (1995).
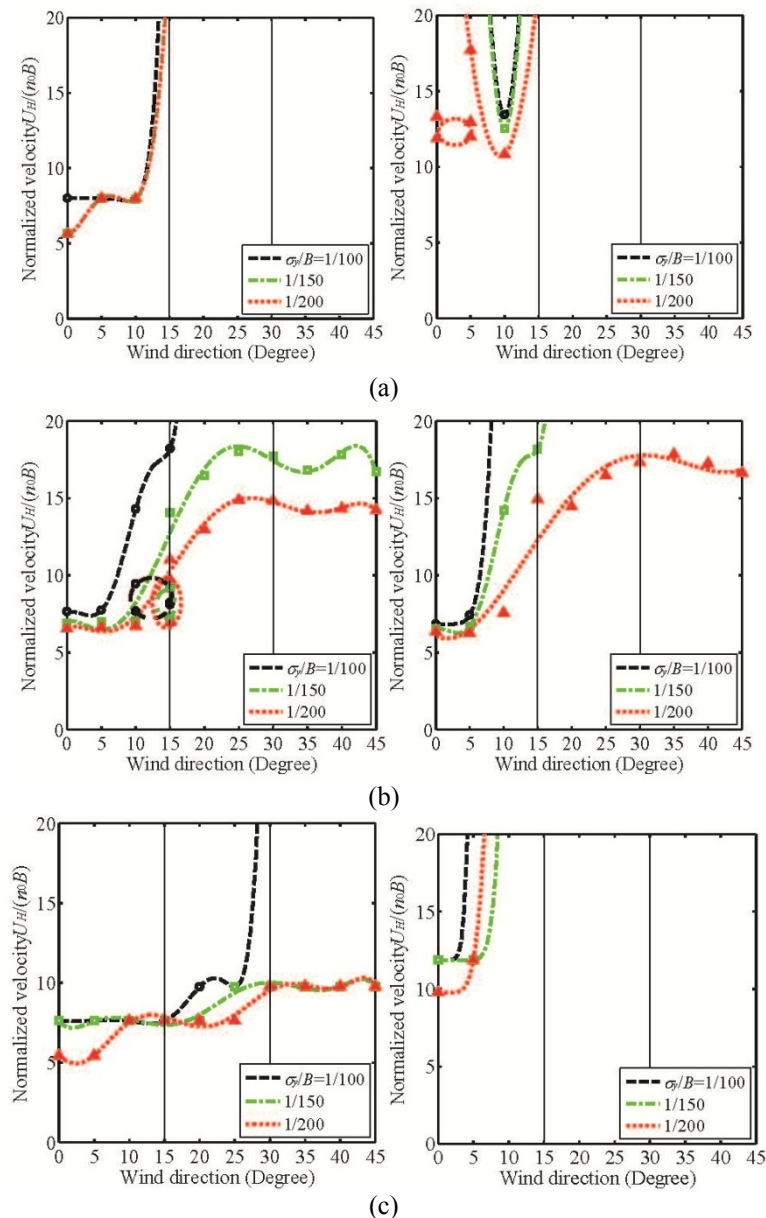

Fig. 8 Stability diagram of normalized response in *Y* direction (Left is for the square model and right is for the tapered model) (a) Low-turbulence flow, (b) Grid-generated flow and (c) Boundary-layer flow
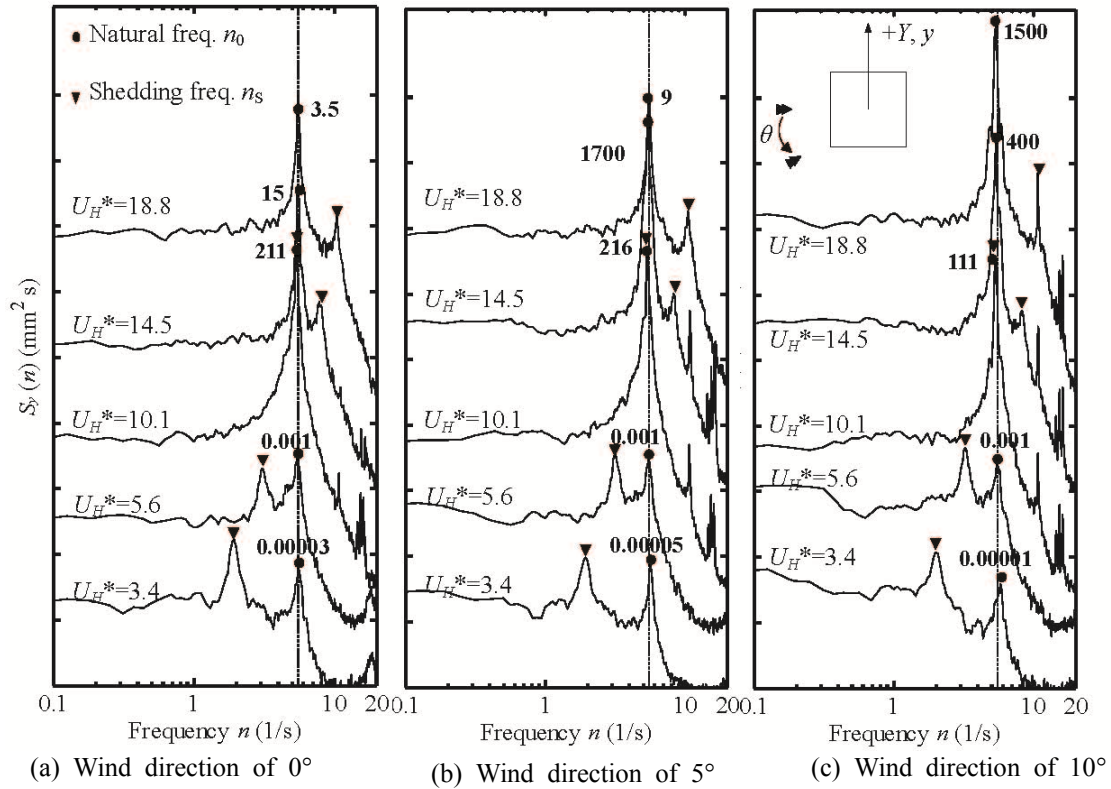
Fig. 9 Power spectra of response in *Y* direction for square model in low-turbulence flow for various wind directions (Values near peak at natural frequency are powers of peaks)

Fig. 11 shows the power spectra for the boundary-layer flow for the wind direction of 0°. Before lock-in excitation, two peaks are observed, and no the shedding frequencies are found after the lock-in excitation. The suppressions of peaks by vortex shedding and broadness of power spectra for the tapered model are easily seen in Fig. 9-11 (Kim and Kanda 2010).

For the power spectra for the grid-generated flow which are not shown here, the shedding frequencies increase with the normalized velocities as in the case of low-turbulence flow, but lock-in is observed at lower normalized velocity as shown in Fig. 12. For the square model for wind direction 0°, as large normalized responses were observed at wide ranges of normalized velocity (Fig. 3(b)), large spectral peaks are also observed for the same normalized velocity range, and these are much larger than those for the low-turbulence flow. Especially for the tapered model, the spectral values are much larger than those for the square model when the normalized velocity is larger than 14.

The values of the normalized shedding frequency n_s/n_0 identified from the spectral peaks are plotted in Fig. 12 and 13 in terms of normalized velocity for the grid-generated flow and boundary-layer flow for small wind directions. It is possible to recognize the clear lock-in range where the shedding frequency n_s is close to the natural frequency n_0, deviating from the linear increasing trend. For the grid-generated flow (Fig. 12), the lock-in range starts near the normalized

velocity of $U_H^*\approx8$ for the square and tapered model, and the lock-in range of the tapered model is roughly three times larger than that of the square model. According to Ukeguchi *et al.* (1970), the lock-in range strongly depends on the response levels i.e., the larger lock-in range was found for the larger responses. As the responses of the tapered model are larger than those of the square model as shown in Fig. 3(b) and 4(b), the larger lock-in range was found for the tapered model.

For the boundary-layer flow (Fig. 13), the lock-in of the tapered model started near the normalized velocity of $U_H^*\approx7$, which is smaller than that of the square model ($U_H^*\approx9$). This is quite interesting result, and for the tapered model in the boundary-layer flow, it can be imagined that the resonances by vortex-shedding at some part of height of the tapered model occur at lower wind speed. This is partly consistent with the result that the spectral value of 1-year return period of the tapered model is larger than that of the square model as pointed out by Tanaka *et al.* (2012).

There exists a relatively small of lock-in range in the low-turbulence flow.

The lock-in excitation in low-turbulence flow was found near the normalized velocity of $U_H^*\approx10$ for both models (partly understood from Fig. 10), and considering the normalized velocities at which the lock-in excitation started for the grid-generated flow and boundary-layer flow, by introducing a moderate turbulence intensity (grid-generated flow), the normalized velocity at which the lock-in excitation started decreased for both models, but by introducing the slopes in mean wind speed and turbulence intensity (boundary-layer flow), the normalized velocity at which the lock-in excitation started increases for the square model and decreases for the tapered model.
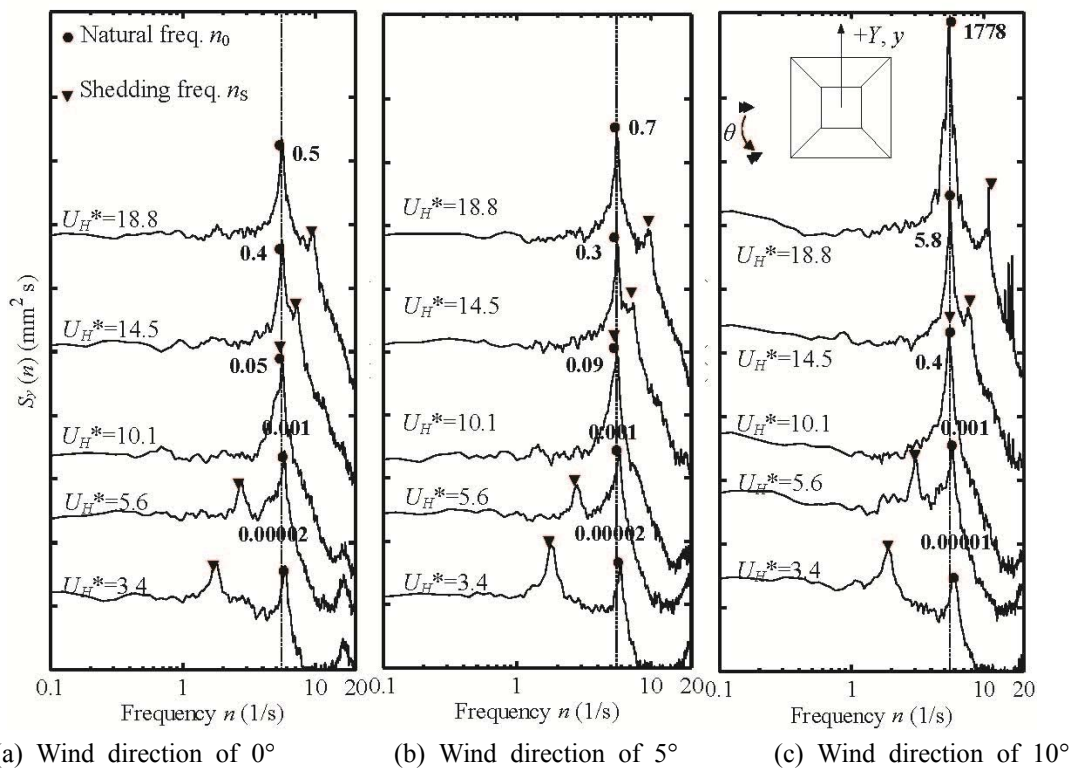

Fig. 10 Power spectra of response in *Y* direction for tapered model in low-turbulence flow for various wind directions (Values near peak at natural frequency are powers of peaks)
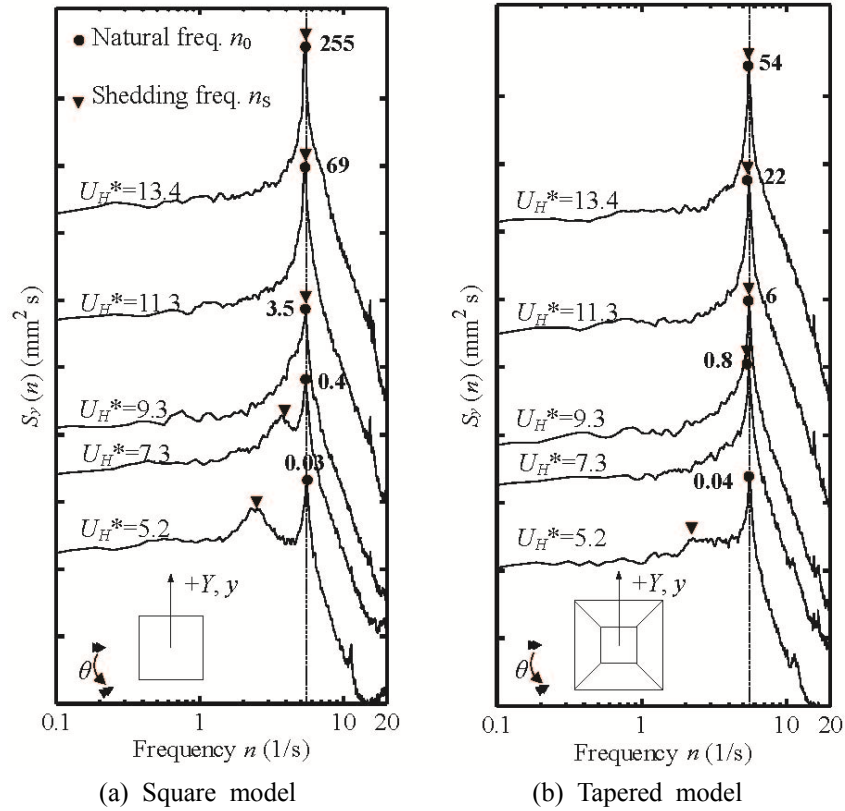
Fig. 11 Power spectra of response in *Y* direction in boundary-layer flow for wind direction of 0°
(Values near peak at natural frequency are powers of peaks)

3.5 Probability function of tip displacement

The probability functions of tip displacements were examined, and it was found that the shape of probability functions can be divided into three types; one is a normal distribution (called Type I), another is a lognormal distribution (called Type II), and the other is a rather strange shape (called Type III) as shown in Fig. 14 together with corresponding time histories. The shapes of probability functions become different depending on the normalized velocities, wind directions, and building shapes, and Tables 2 and 3 summarize the types of the probability functions.

In a low-turbulence flow in Table 2, for the square model in the *X* direction (σ_x/B) mostly Type I (Normal distribution) and Type II (Lognormal distribution) were observed for the responses, and Type III was only observed at $U_H{}^*$=12.3 for the wind direction of 0°. Type II was observed before and after the lock-in excitations, and for wind directions larger than 20° only Type I was observed. On the other hand Type I and Type III were observed in the *Y* direction (σ_y/B), and Type III was found mostly in the normalized velocities where the vortex-induced vibrations occur for the wind directions of 0° ~ 10°. For other wind directions, Type I was found. For the tapered model, Type III was shown only for the normalized velocity of $U_H{}^*$=18.8 for the wind direction of 10°.
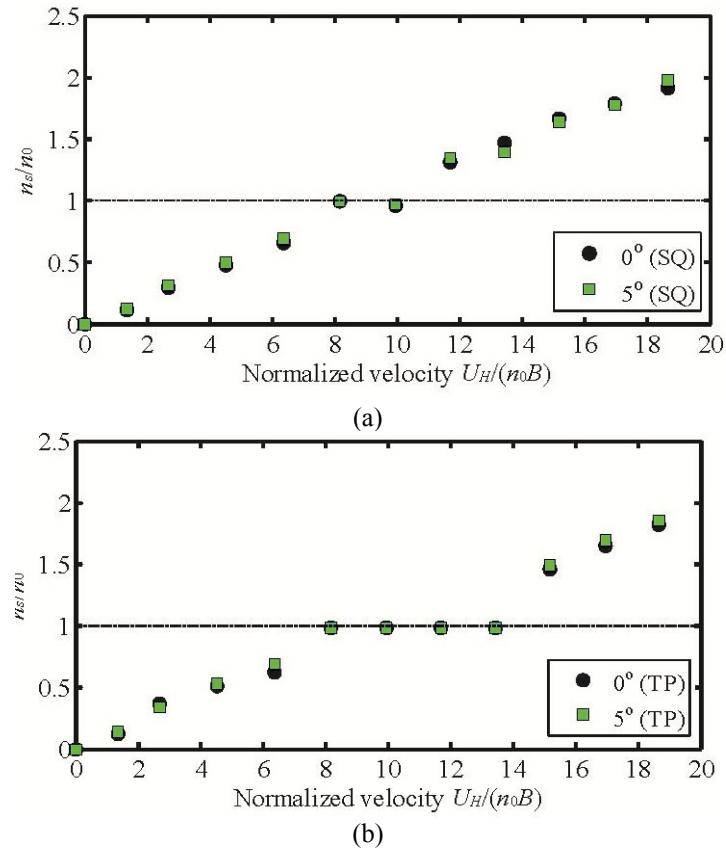
Fig. 12 Variations of shedding frequencies in grid-generated flow (a) Square model, (b) Tapered model

In the grid-generated flow in Table 3, only Type I was observed for all the normalized velocities and wind directions for the square and tapered model in the X direction (σ_x/B). For the responses in the Y direction (σ_y/B), Type III was found for the wind directions of 0° and 5° for both models, but the normalized velocity where Type III was observed was small for the tapered model.

Only Type I was found in the boundary-layer flow for the square and tapered model in the X and Y directions.

Figs. 15 shows the relationship between the normalized response in the Y direction and corresponding time histories, power spectra and probability functions for the square model (SQ, θ=5°) and tapered model (TP, θ=10°) in low-turbulence flow. Clear differences in time histories, shape of power spectra and probability functions were found depending on the levels of responses of the experimental models. At the normalized velocities for the largest normalized responses, although the shedding frequencies do not coincide with the natural frequencies, their spectral peaks are much larger than other peaks. This larger peak gives a larger normalized response, and it is assumed to associate with the decrease in aerodynamic damping ratios as pointed out by Kawai (1998).
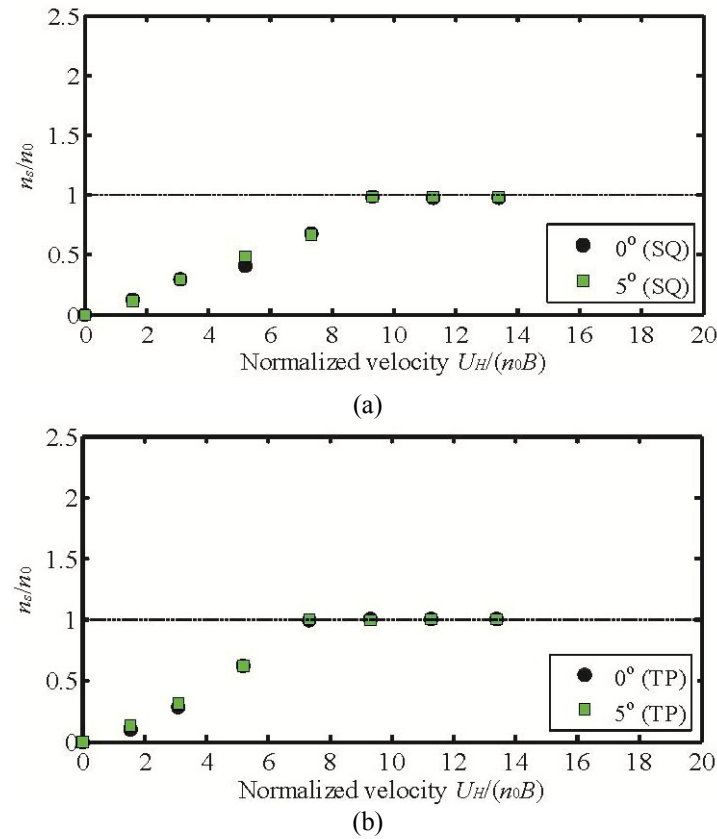
Fig. 13 Variations of shedding frequencies in boundary-layer flow (a) Square model, (b) Tapered model

5. Conclusions

Using conventional square and tapered super-tall building models, aeroelastic wind tunnel experiments were conducted to investigate the effect of taper on fundamental aeroelastic behaviors in terms of normalized responses, power spectra, stability diagrams, probability functions, and so on.

In low-turbulence flow, strong vortex-induced vibrations occurred for the square model for small wind directions, but vortex-induced vibrations were greatly suppressed by introducing taper. But for the tapered model, large vortex-induced vibrations were still observed for a specific wind direction. Moderate turbulence in the incident flow (grid-generated flow) changes significantly the condition of vortex-induced vibration, showing large responses for wide ranges of the normalized velocity for small wind directions.

And it was interesting that suppression of responses by introducing taper cannot be expected in the grid-generated flow. In the boundary-layer flow with slopes in mean wind speed and turbulence intensity, the responses become much smaller than other flow conditions, and no vortex-induced

vibrations were observed in the current experimental conditions. The responses of the tapered model are much smaller than those of the square model.

From the stability diagram, the unstable region of the square model becomes wider in the order of boundary-layer flow, grid-generated flow and low-turbulence flow, even though large responses were found in grid-generated flow and low-turbulence flow. For the tapered model, the stability diagram is very sensitive to the conditions of incident flows, showing a totally different trend to the square model.
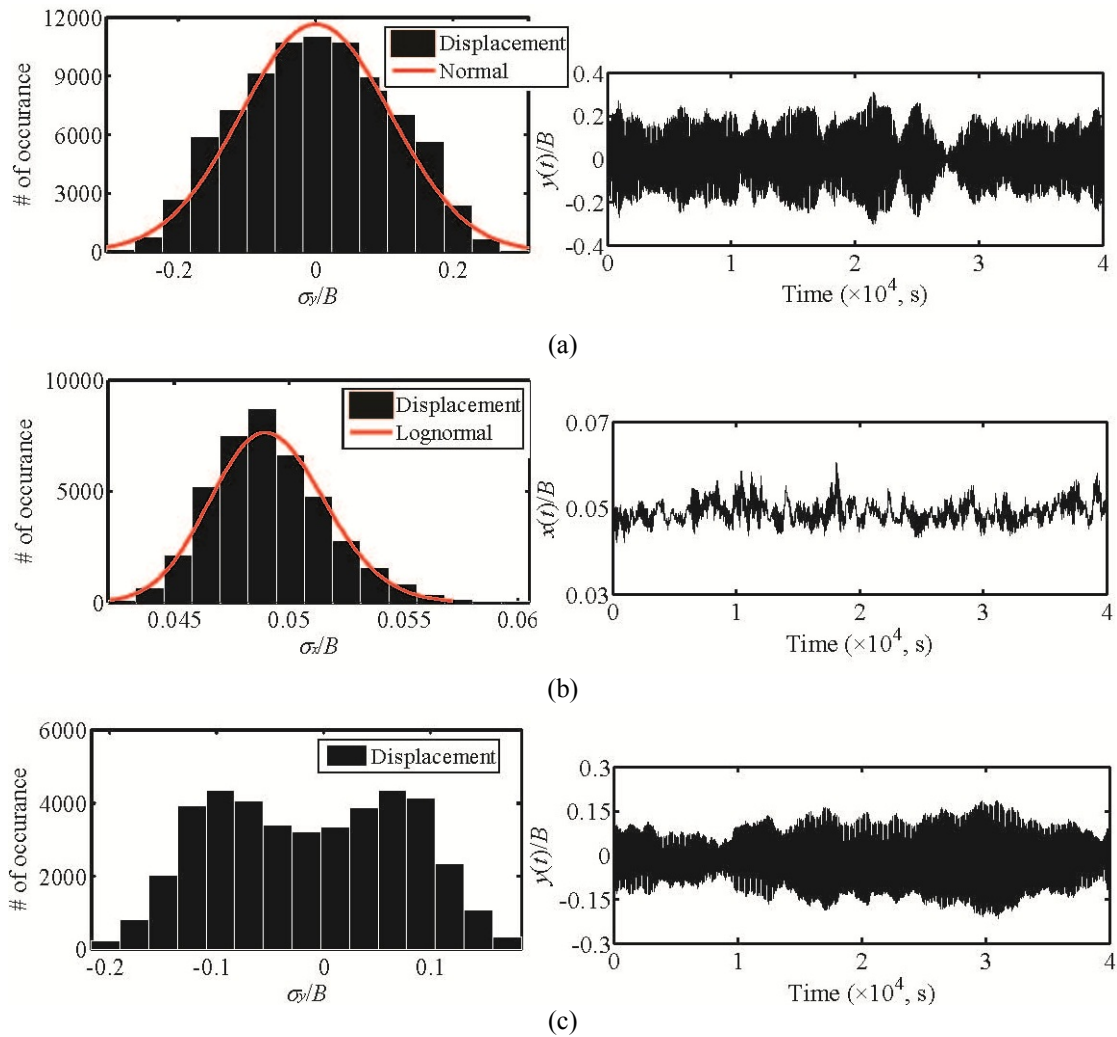

Fig. 14 Probability function and time history of tip displacement (a) Type I (Normal distribution, Square model, Boundary-layer flow, $\theta=0°$, $U_H^*=13.4$), (b) Type II (Lognormal, Square model, Low-turbulence flow, $\theta=0°$, $U_H^*=16.7$), (c) Type III (Tapered model, Grid-generated flow, $\theta=5°$, $U_H^*=18.6$)
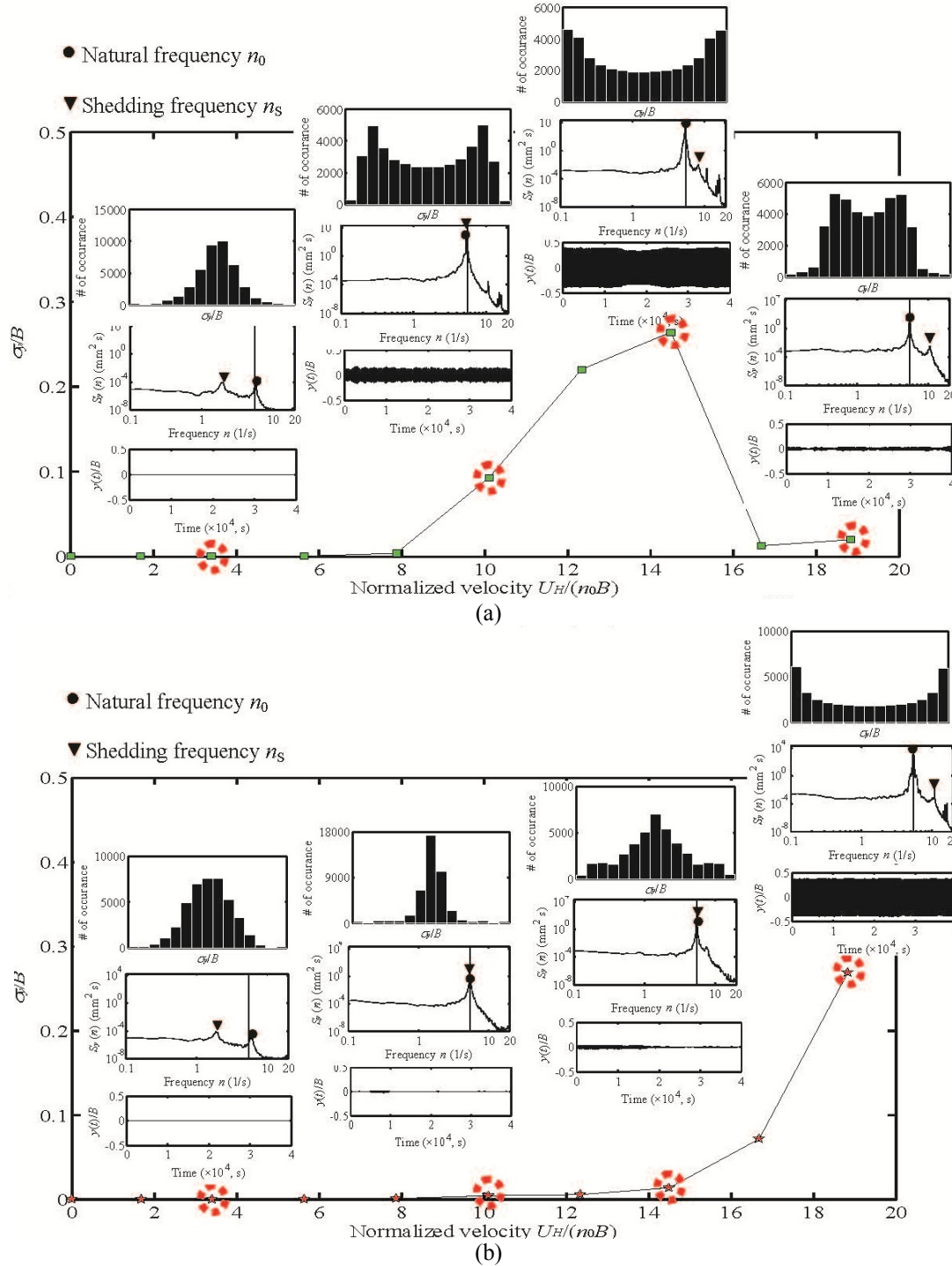
Fig. 15 Response in *Y* direction with time history, power spectrum and probability function in low-turbulence flow (a) Square model ($\theta=5°$), (b) Tapered model ($\theta=10°$)

Table 2 Type of probability function in low-turbulence flow

$U_H{}^*$	Square model										Tapered model					
	0°		5°		10°		15°		20° ~ 45°		0° ~ 5°		10°		15° ~ 45°	
	σ_x/B	σ_y/B	σ_x/B	σ_y/B	σ_x/B	σ_y/B	σ_x/B	σ_y/B	σ_x/B	σ_y/B	σ_x/B	σ_y/B	σ_x/B	σ_y/B	σ_x/B	σ_y/B
3.4			II		II		II									
5.6			II				II									
7.9	II	III	II		II		II									
10.1		III		III	III	III	II									
12.3	III	III		III	III	III										
14.5	II	III		III	III	III										
16.7	II		II	III		III										
18.8	II		II	III		III								III			

Table 3 Type of probability function in grid-generated flow

$U_H{}^*$	Square model						Tapered model					
	0°		5°		10° ~ 45°		0°		5°		10° ~ 45°	
	σ_x/B	σ_y/B	σ_x/B	σ_y/B	σ_x/B	σ_y/B	σ_x/B	σ_y/B	σ_x/B	σ_y/B	σ_x/B	σ_y/B
2.7												
4.5												
6.4												
8.2								III				
9.9		III						III				
11.7		III						III		III		
13.4		III		III				III		III		
15.2		III		III				III		III		
16.9		III		III				III		III		
18.6		III		III				III		III		

☐ Type I (Normal distribution)
▨ Type II (Lognormal distribution)
▩ Type III

Lock-in regions were identified from the peak of power spectra, and the normalized velocity at which the lock-in excitation started and the range of the normalized velocities where the lock-in excitation was observed were strongly dependent on the building shape and incident flow conditions. A wide range of lock-in excitations were observed for the tapered model for grid-generated flow and boundary-layer flow.

The shapes of the probability functions can be divided into three types. Type II (Lognormal distribution) was only found for the square model in the X direction in low-turbulence flow, and Type III were mostly observed at high normalized velocities and small wind directions, where the vortex-induced vibrations were observed, in low-turbulence flow and grid-generated flow. In the boundary-layer flow, only Type I (Normal distribution) was found.

Acknowledgments

References

Architectural Institution of Japan (2004), *Recommendations for Loads on Buildings (2004)*, Architectural Institution of Japan, Tokyo.

Belloli, M., Fossati, F., Giappino, S., Muggiasca, S. and Villani, B. (2011), "On the aerodynamic and aeroelastic response of a bridge tower", *J. Wind Eng. Ind. Aerod.*, **99**(6-7), 729-733.

Belloli, M., Rosa, L. and Zasso, A. (2014), "Wind loads and vortex shedding analysis on the effects of the porosity on a high slender tower", *J. Wind Eng. Ind. Aerod.*, **126**, 75-86.

Carassale, L, Freda, A. and Marrè-Brunenghi, M. (2013), "Effects of free-stream turbulence and corner shape on the galloping instability of square cylinders", *J. Wind Eng. Ind. Aerod.*, **123**, 274-280.

Huang, P., Quan, Y. and Gu, M. (2013), "Experimental study of aerodynamic damping of typical tall buildings", *Math. Problems Eng.*, **2013**, 1-9.

John, A. D., Gairola, A., Ganju, E. and Gupta, A. (2011), "Design wind loads on reinforced concrete chimney - An experimental case study", *Procedia Eng.*, **14**, 1252-1257.

Kawai, H. (1995), "Effects of angle of attack on vortex induced vibration and galloping of tall buildings in smooth and turbulent boundary layer flows", *J. Wind Eng. Ind. Aerod.*, **54-55**, 125-132.

Kawai, H. (1998), "Effect of corner modifications on aeroelastic instabilities of tall buildings", *J. Wind Eng. Ind. Aerod.*, **74-76**, 719-729.

Kim, Y. and Kanda, J. (2010), "Effects of taper and setback on wind force and wind-induced response of tall buildings", *Wind Struct.*, **13**(6), 499-517.

Kim, Y.C. and Kanda, J, (2013), "Wind pressures on tapered and set-back tall building", *J. Fluid. Struct.*, **39**, 306-321.

Kim, Y.M., You, K.P. and Ko, N.H. (2008), "Across-wind responses of an aeroelastic tapered tall building", *J. Wind Eng. Ind. Aerod.*, **96**(8-9), 1307-1319.

Kwok, K.C.S. and Melbourne, W.H. (1980), "Free stream turbulence effects on galloping", *J. Eng. Mech. Div.*, **106**(2), 273-288.

Naudascher, E. and Rockwell, D. (2005), *Fluid-induced vibrations, An engineering guide*, Dover Publication, INC., New York.

Novak, M. and Davenport, A.G. (1970), "Aeroelastic instability of prisms in turbulent flow", *J. Eng. Mech. Div.*, **96**(1), 17-39.

Parkinson,G.V. and Smith, J.D. (1964), "The square prism as aeroelastic non-linear oscillator", *Q. J. Mech. Appl. Math.*, **17**(2), 225-239.

Pozzuoli C., Bartoli, G., Peil, U. and Clobes, M. (2013), "Serviceability wind risk assessment of tall buildings including aeroelastic effects", *J. Wind Eng. Ind. Aerod.*, **123**, 325-338.

Tamura, Y. (2012), "Amplitude dependency of damping in buildings and critical tip drift ratio", *Int. J. High-Rise Build.*, **1**, 1-13.

Tanaka, H., Tamura, Y., Ohtake, K., Nakai, M. and Kim, Y.C. (2012), "Experimental investigation of aerodynamic forces and wind pressures acting on tall buildings with various unconventional configurations", *J. Wind Eng. Ind. Aerod.*, **107-108**, 179-191.

Tanaka, H., Tamura, Y., Ohtake, K., Nakai, M. and Kim, Y.C. (2013), "Aerodynamic and Flow Characteristics of Tall Buildings with Various Unconventional Configurations", *Int. J. High-Rise Build.*, **2**(3), 213-228.

Ukeguchi, N., Tanaka, H., Takahara, S. and Matsui, Y. (1970), "Study on unsteady aerodynamic forces acting on an oscillating circular cylinder", *Proceedings of the 1st Natl. Symp. Wind Eng.*, 153-160 (In Japanese).

CC